Athens Institute for Education and Research
ATINER

ATINER's Conference Paper Series
MEC2019-2671

Aircraft Dynamic Stability & Control Analysis for an Advanced Military Trainer Conceptual Design

Royd Johansen
MSc Student
San José State University
USA

Nikos Mourtos
Professor
San José State University
USA

An Introduction to

ATINER's Conference Paper Series

Conference papers are research/policy papers written and presented by academics at one of ATINER's academic events. ATINER's association started to publish this conference paper series in 2012. All published conference papers go through an initial peer review aiming at disseminating and improving the ideas expressed in each work. Authors welcome comments.

Dr. Gregory T. Papanikos
President
Athens Institute for Education and Research

This paper should be cited as follows:

Johansen, R. and Mourtos, N. (2019). **"Aircraft Dynamic Stability & Control Analysis for an Advanced Military Trainer Conceptual Design",** Athens: ATINER'S Conference Paper Series, No: **MEC2019-2671.**

Athens Institute for Education and Research
8 Valaoritou Street, Kolonaki, 10671 Athens, Greece
Tel: + 30 210 3634210 Fax: + 30 210 3634209 Email: info@atiner.gr URL: www.atiner.gr
URL Conference Papers Series: www.atiner.gr/papers.htm

ISSN: 2241-2891
02/10/2019

Aircraft Dynamic Stability & Control Analysis for an Advanced Military Trainer Conceptual Design

Royd Johansen
Nikos Mourtos

Abstract

Dynamic analysis provides valuable feedback to designers to validate design choices. The following discusses a top-level approach for developing a state-space for an aircraft and the five general flight modes. The conceptual aircraft used for the analysis was developed through an aircraft design project based on an advanced military trainer for the USAF T-X Program. The condition for analysis was evaluated at cruise. The results showed a typical longitudinal response in the phugoid and short period modes, and an unstable divergent spiral in the lateral/directional response.

Keywords: Aircraft, Design, Dynamic Modes, Stability and Control.

Introduction

In 2003 the United States Air Force (USAF) began developing requirements for a new aircraft program called the T-X program. The purpose of the T-X program was to replace the existing advanced trainer, the T-38 Talon, and upgrade the current advanced flight program to meet the demands of the USAF's modern and future aircraft. The T-38 is an aging supersonic advanced trainer developed in the 1950s, that cannot meet the USAF's demands as an advanced trainer. Due to budget constraints and other higher priority programs, the official request for formal T-X program proposals from the aerospace industry didn't occur until 2016. Top aerospace companies planning to submit proposal were Boeing/Saab, Lockheed Martin/Korean Aerospace Industries, Northrop Grumman, Leonardo, and Sierra Nevada Corporation. Ultimately the decision came down to the partnerships of Boeing/Saab and Lockheed Martin/Korean Aerospace Ind. At the end of September 2018, the USAF awarded the T-X program contract to the Boeing-Saab partnership (Figure 1).

Figure 1. *Boeing/Saab T-X Prototype Aircraft*

In August 2018, a conceptual aircraft design project [1] began based off the T-X program requirements for an advanced military trainer (AMT). The design process included configuration selection, weight sizing, performance sizing, fuselage design, wing design, empennage design, landing gear design, weight and balance, static longitudinal and directional stability, and drag polars [2]. This initial conceptual design was then further explored using Class II methods, such as supersonic area ruling and drag polar approximations, V-n diagrams, Class II weight and balance, moments and products of inertia, and cost estimation. The resulting model from the design process is shown in Figure 2.

Figure 2. *AMT Conceptual Design Model*

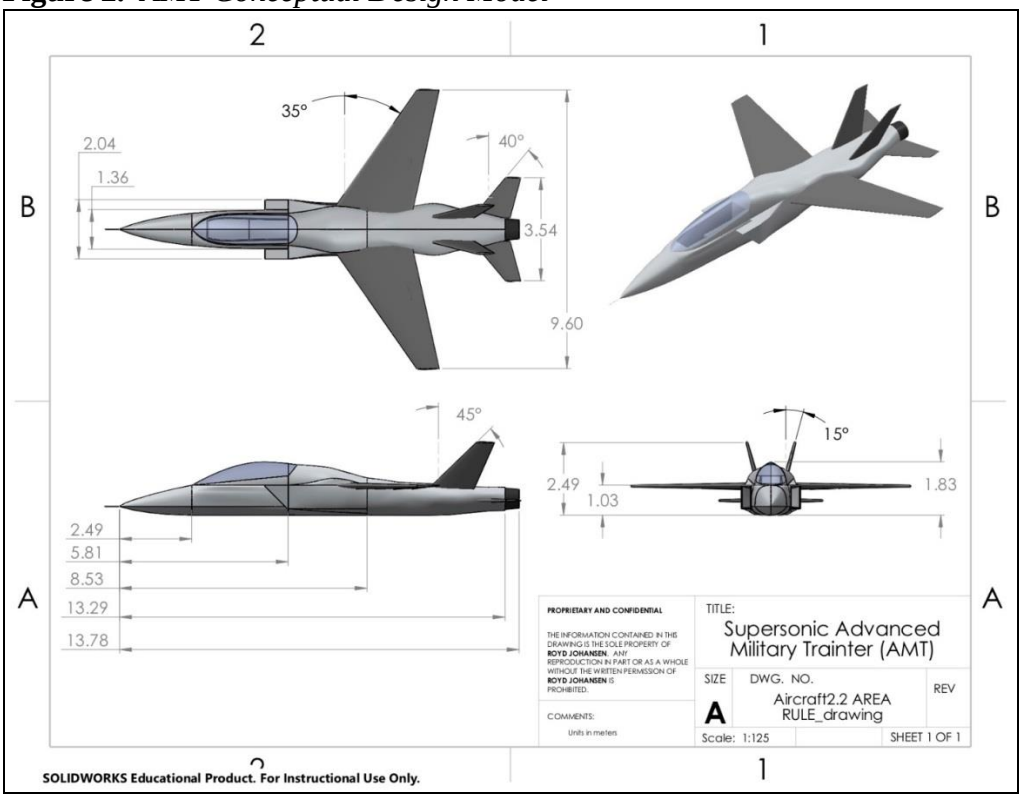

The purpose of the following work is to develop a Matlab code for determining the longitudinal and lateral/directional response of the conceptual aircraft. The only input requirements for the code are the state-space dynamic derivatives. Therefore, the code can be used for any aircraft to evaluate the time domain response of the longitudinal and lateral/directional modes. The only exception is the lateral/directional state-space is developed for an aircraft with a negligible XZ product of inertia.

The analysis completed is for steady-state cruise of Mach 0.7. The longitudinal analysis is focused on the short-period and phugoid modes. The lateral-directional analysis is to determine what types of modes the AMT may have: dutch-roll, spiral divergence, and/or roll divergence.

Methodology

Reference Frames and Symbolic Notation

The body reference frame for an aircraft is defined in Figure 3. Where, the x-direction is out the nose, the y-direction is along the starboard wing, and the z-direction is down. The body reference frame is related to the Earth's surface fixed reference frame through the Euler angles of yaw (Ψ), pitch (Θ), and roll (Φ).

Figure 3. *Fixed and Body Frame [3]*

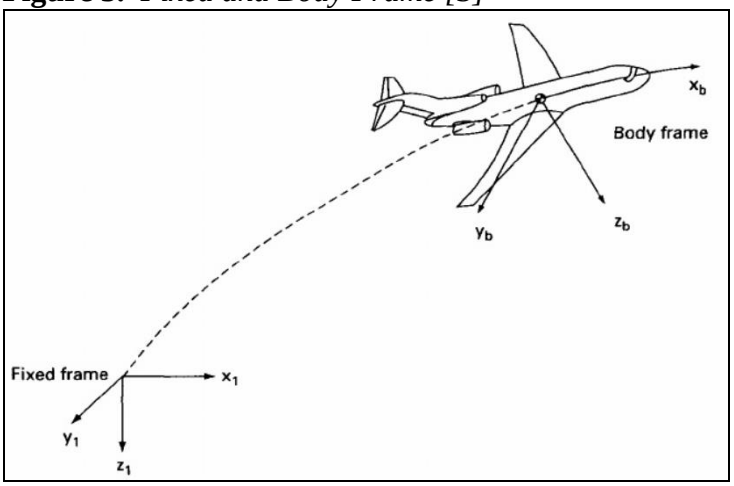

The various components of flight parameters that are used in the following sections use the notation shown in Table 1

Table 1, which can be seen visually in Figure 4. The notation for command inputs is the following: elevator (δe), aileron (δa), rudder (δr), and thrust (δT). The design does not utilize conventional elevator for pitch control, but a stabilator or flying tail. Therefore, the elevator notation used is to be consistent with conventional stability and control used in literature. The notation for derivatives is with a subscript, for example $\partial X/\partial u = X_u$. Multiple subscripts or other notations used in the following sections are described in context.

Table 1. *Airplane Component Flight Parameters*

Parameter	x-direction	y-direction	z-direction
Linear Velocity	U	V	W
Perturbed Velocity	u	v	w
Angular Velocity	P	Q	R
Perturbed Angular Velocity	p	q	r
Euler Angle	Φ	Θ	Ψ
Perturbed Euler Angle	ϕ	θ	ψ
Force	X	Y	Z
Moment	$\mathcal{L}$	$\mathcal{M}$	$\mathcal{N}$

Figure 4. *Directional Notation for Velocity, Angular Velocity, Forces, and Moments [3]*

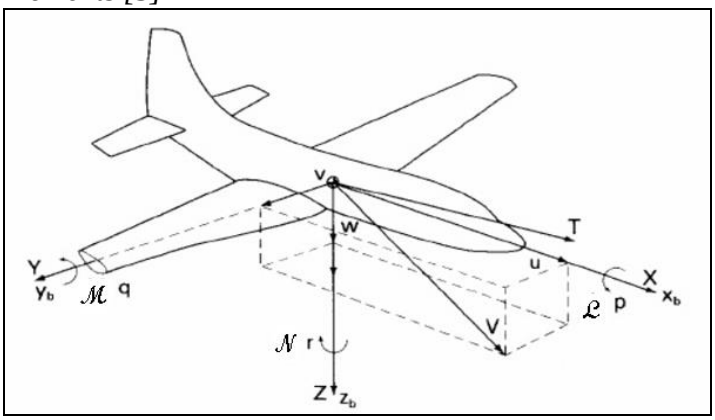

Equations of Motion

This section discusses how fundamental laws are used to develop the state space and transfer functions used to perform analysis on aircraft dynamics. For the derivation of the equations of motion, state space, and transfer functions, references [3], [4], and [5] may be consulted.

The equations of motion are developed from Newtons second law for forces and moments.

$$\sum \text{Forces} = \frac{\mathrm{d}}{\mathrm{dt}}(\mathrm{m} \cdot \text{velocity}), \quad \sum \text{Moments} = \frac{\mathrm{d}}{\mathrm{dt}}\mathrm{H}$$

The vector equations of motion are developed in the body-frame and are transformed to the fixed-frame through the Euler angles. Examples of this transformation can be found in chapter 3 [3], chapter 1 [4], or chapter 4 [5]. In the equations of motion, the only forces being considered are aerodynamic, propulsive, and gravitational.

The general equations of motion are non-linear. To linearize the equations, small-disturbance theory is used [3], [4], and [5]. This theory assumes that any deviation in motion from a steady-state flight conditions is small, such that the linear and angular velocities can be written as a sum of the steady-state condition (U, V, W, P, Q, and R) and a small change (u, v, w, p, q, and r). This theory also assumes the following:

$$V = W = P = Q = R = \Phi = \Psi = 0$$

The last assumption is the small angle approximation, which reduces sine and cosine terms to angles in radians. These trigonometry terms are a resultant of transforming the vectors in the body-frame to the fixed frame. The equations of motion are divided into the longitudinal equation (1) and lateral equations (2) [3].

$$\begin{gathered}\dot{u} - X_u \cdot u - X_w \cdot w + g \cdot \theta = X_{\delta e} \cdot \delta e + X_{\delta T} \cdot \delta T \\ -Z_u \cdot u + (1 - Z_{\dot{w}})\dot{w} - Z_w \cdot w - (U + Z_q)\dot{\theta} = Z_{\delta r} \cdot \delta r + Z_{\delta T} \cdot \delta T \\ \underbrace{-\mathcal{M}_u \cdot u - \mathcal{M}_{\dot{w}} \cdot \dot{w} - \mathcal{M}_w \cdot w + \ddot{\theta} - \mathcal{M}_q \cdot \dot{\theta} = \mathcal{M}_{\delta r} \cdot \delta r + \mathcal{M}_{\delta T} \cdot \delta T}_{longitudinal}\end{gathered} \tag{1}$$

$$\begin{gathered}v - Y_v \cdot v - Y_p \cdot p + (U - Y_r)r - g \cdot \phi = Y_{\delta r} \cdot \delta r \\ -\mathcal{L}_v \cdot v + \dot{p} - \mathcal{L}_p \cdot p - \frac{I_{yz}}{I_{xx}}\dot{r} - \mathcal{L}_r \cdot r = \mathcal{L}_{\delta a} \cdot \delta a + \mathcal{L}_{\delta r} \cdot \delta r \\ \underbrace{-\mathcal{N}_v \cdot v - \frac{I_{xz}}{I_{zz}}\dot{p} + \mathcal{N}_p \cdot p + \dot{r} - \mathcal{N}_r \cdot r = \mathcal{N}_{\delta a} \cdot \delta a + \mathcal{N}_{\delta r} \cdot \delta r}_{lateral}\end{gathered} \tag{2}$$

Longitudinal Dynamics

The state-space of the longitudinal dynamics is determined using the longitudinal equations of motion, equations (1). The general state-space form is the following:

$$\dot{\vec{x}} = [A]\vec{x} + [B]\vec{u}$$

Where, x is the state-space vector, A and B are the aircraft stability derivatives, and u is the control vector.

There are assumptions necessary to simplify the equations. The first assumption is the state-space is for a rigid aircraft body that does not consider elastic effects, such as the wings bending due to the lift. The second assumption is that $Z_{\dot{w}}$ and Z_q are zero because these derivatives are generally small [3]. The additional state $\dot{\theta} = q$ is added to form a square A-matrix.

The analysis that will be performed will only be for the dynamic response due to elevator inputs, therefore δT will not be used. The resulting longitudinal equations of motion are transformed to the state-space notation shown with equation (3). Other assumptions or states could be used to develop a different state-space. Equation (3) is simply the states of interest for the longitudinal dynamics.

$$\begin{bmatrix} \dot{u} \\ \dot{w} \\ \dot{q} \\ \dot{\theta} \end{bmatrix} = \begin{bmatrix} X_u & X_w & 0 & -g \\ Z_u & Z_w & U & 0 \\ (\mathcal{M}_u + \mathcal{M}_{\dot{w}}Z_u) & (\mathcal{M}_w + \mathcal{M}_{\dot{w}}Z_w) & (\mathcal{M}_q + \mathcal{M}_{\dot{w}}U) & 0 \\ 0 & 0 & 1 & 0 \end{bmatrix} \begin{bmatrix} u \\ w \\ q \\ \theta \end{bmatrix} + \begin{bmatrix} X_{\delta e} \\ Z_{\delta e} \\ (\mathcal{M}_{\delta e} + \mathcal{M}_{\dot{w}}Z_{\delta e}) \\ 0 \end{bmatrix} [\delta e] \tag{3}$$

Longitudinal Derivatives

The longitudinal stability and elevator control derivatives are mathematically defined in equations (4) through (14) [3], [4], and [6]. In the equations there is

notation that has not been previously defined. The freestream dynamic pressure ($\bar{q}_\infty$) is accented with an over bar so as not to be confused with the perturbed pitch rate (q). The other three notations are for mass (m), wing area (S), and wing mean aerodynamic chord ($\bar{c}$). In cases where there is a second subscript, this is due to the capital C to imply a non-dimensional coefficient. For example, C_{D_U} is the variation in airplane drag due to change in forward velocity. A third subscript indicates an object, for example A/C is for aircraft.

Forward Acceleration per Unit Change in Forward Velocity

$$X_u = -\frac{\bar{q}_\infty \cdot S\left(C_{D_U} + 2C_{D_1}\right)}{m \cdot U_1} \quad \left(\frac{1}{sec}\right) \tag{4}$$

Forward Acceleration per Unit change in Vertical Velocity

$$X_w = -\frac{\bar{q}_\infty \cdot S\left(C_{D_\alpha} - C_{L_1}\right)}{m \cdot U_1} \quad \left(\frac{1}{sec}\right) \tag{5}$$

Forward Acceleration per Unit Elevator Deflection Angle

$$X_{\delta e} = -\frac{\bar{q}_\infty \cdot S \cdot C_{D_{\delta e}}}{m} \quad \left(\frac{ft/sec^2}{rad}\right) or \left(\frac{m/sec^2}{rad}\right) \tag{6}$$

Vertical Acceleration per Unit Change in Forward Velocity

$$Z_u = -\frac{\bar{q}_\infty \cdot S\left(C_{L_u} + 2C_{L_1}\right)}{m \cdot U_1} \quad \left(\frac{1}{sec}\right) \tag{7}$$

Vertical Acceleration per Unit change in Vertical Velocity

$$Z_w = -\frac{\bar{q}_\infty \cdot S\left(C_{L_{\alpha_{A/C}}} + C_{D_1}\right)}{m \cdot U_1} \quad \left(\frac{1}{sec}\right) \tag{8}$$

Vertical Acceleration per Unit Elevator Deflection Angle

$$Z_{\delta e} = \frac{\bar{q}_\infty \cdot S \cdot C_{Z_{\delta e}}}{m} \quad \left(\frac{ft/sec^2}{rad}\right) or \left(\frac{m/sec^2}{rad}\right) \tag{9}$$

Pitch Angular Acceleration per Unit Change in Forward Velocity

$$\mathcal{M}_u = \frac{\bar{q}_\infty \cdot S \cdot \bar{c} \cdot C_{\mathcal{M}_u}}{I_{yy} \cdot U_1} \quad \left(\frac{rad}{ft \cdot sec}\right) or \left(\frac{rad}{m \cdot sec}\right) \tag{10}$$

Pitch Angular Acceleration per Unit Change in Vertical Acceleration

$$\mathcal{M}_{\dot{w}} = \frac{\bar{q}_\infty \cdot S \cdot \bar{c}^2 \cdot C_{\mathcal{M}_{\dot{\alpha}}}}{2I_{yy} \cdot U_1^2} \quad \left(\frac{1}{ft}\right) or \left(\frac{1}{m}\right) \tag{11}$$

Pitch Angular Acceleration per Unit Change Vertical Velocity

$$\mathcal{M}_w = \frac{\bar{q}_\infty \cdot S \cdot \bar{c} \cdot C_{\mathcal{M}_\alpha}}{I_{yy} \cdot U_1} \quad \left(\frac{rad}{ft \cdot sec}\right) or \left(\frac{rad}{m \cdot sec}\right) \tag{12}$$

Pitch Angular Acceleration per Unit Pitch Rate

$$\mathcal{M}_q = \frac{\bar{q}_\infty \cdot S \cdot \bar{c}^2 \cdot C_{\mathcal{M}_q}}{2I_{yy} \cdot U_1} \quad \left(\frac{1}{sec}\right) \tag{13}$$

Pitch Angular Acceleration per Unit Elevator Deflection Angle

$$\mathcal{M}_{\delta e} = \frac{\bar{q}_\infty \cdot S \cdot \bar{c} \cdot C_{\mathcal{M}_{\delta e}}}{I_{yy}} \quad \left(\frac{1}{sec^2}\right) \tag{14}$$

The longitudinal stability and control derivatives are those defined for the state-space above. Depending on the state-space developed for an aircraft's analysis additional or other derivatives may be required [3], [4], and [6].

Longitudinal Coefficients

The longitudinal coefficients required for the above stability and control derivatives are mathematically expressed with equations (15) through (26) [3], [4], and [6]. Generally, the Mach number is indicated with a capital M. To reduce confusion, M# is used in the following equations. In most aerodynamics or aircraft books capital A is used to represent aspect ratio, but in the following equations AR is used for better clarity. Oswald efficiency is still (e). The dynamic pressure ratio of the horizontal tail is $\eta_H = \bar{q}_H/\bar{q}_\infty$. Since the wing creates downwash on the tail, the airflow the horizontal sees is not the same as the freestream, which is the reason for this correction. The other notations not previously defined are the downwash gradient ($\partial\varepsilon/\partial\alpha$) and control surface to lifting surface area ratio ($\tau_{\delta e}$).

Variation in Airplane Drag Coefficient with Dimensionless Forward Velocity

$$C_{D_u} = M\# \cdot \frac{\partial C_D}{\partial M\#} \tag{15}$$

This coefficient is generally zero for subsonic Mach numbers. An aircraft that flies in the transonic and/or supersonic regions will have a significant C_{D_u} due to compressibility effects of wave drag, see Figure 5.

Figure 5. *Mach Effect on Drag Coefficient [6]*

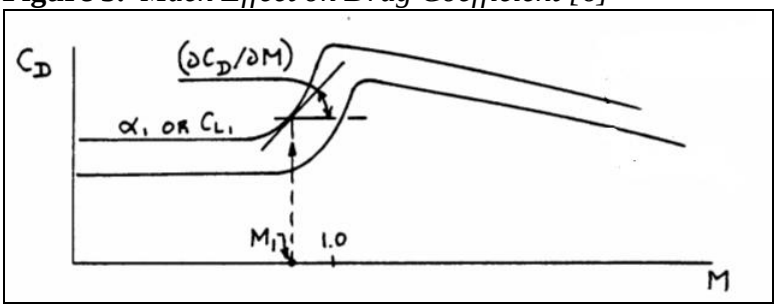

Variation in Airplane Drag Coefficient with Angle of Attack

$$C_{D_\alpha} = \frac{2C_{L_1}}{\pi \cdot e \cdot AR} C_{L_{\alpha_{A/C}}} \tag{16}$$

Variation in Airplane Drag Coefficient with Elevator Deflection Angle

$$C_{D_{\delta e}} = \alpha_{\delta e} \cdot 2C_{L_{\alpha_H}} \cdot \eta_H \cdot \frac{S_H}{S} \cdot \frac{C_{L_o}}{\pi \cdot e \cdot AR} \tag{17}$$

Variation in Airplane Lift Coefficient with Dimensionless Forward Velocity

$$C_{L_u} = \frac{\{M\#_1 \cos(\Lambda_{c/4})\}^2}{1 - \{M\#_1 \cos(\Lambda_{c/4})\}^2} \cdot C_{L_1} \tag{18}$$

Variation in Airplane Lift

$$C_{L_{\alpha_{A/C}}} = C_{L_{\alpha_W}} + C_{L_{\alpha_H}} \left(1 - \frac{\partial\varepsilon}{\partial\alpha}\right) \eta_H \frac{S_H}{S} \tag{19}$$

Coefficient with Angle of Attack Variation in Airplane Z-force Coefficient with Elevator Deflection Angle

$$C_{Z_{\delta e}} = -C_{L_{\alpha_H}} \cdot \eta_H \frac{S_H}{S} \quad \left(\frac{1}{\text{rad}}\right) \tag{20}$$

Airplane Pitching Moment Coefficient Variation in Airplane Pitching Moment Coefficient with Forward Velocity

$$C_{\mathcal{M}} = C_{\mathcal{M}_{wb}} - C_{L_w}\left(\bar{x}_{ac_W} - \bar{x}_{CG}\right) - C_{L_H}\left(\bar{x}_{ac_H} - \bar{x}_{CG}\right)\eta_H \frac{S_H}{S} \tag{21}$$

$$C_{\mathcal{M}_U} = M\# \cdot C_L \cdot \frac{\partial x_{ac_{A/C}}}{\partial M\#} \tag{22}$$

The variation in aircraft aerodynamic center with Mach number was determined from previous work while performing static stability and static margin analysis [1].

Variation in Airplane Pitching Moment Coefficient with Angle of Attack Rate Variation in Airplane Pitching Moment Coefficient with Angle of Attack Variation in Airplane Pitching Moment Coefficient with Pitch Rate

$$C_{\mathcal{M}_{\dot{\alpha}}} = -2C_{L_{\alpha_H}}\left(\bar{x}_{ac_H} - \bar{x}_{CG}\right)^2 \left(\frac{\partial \varepsilon}{\partial \alpha}\right)\eta_H \frac{S_H}{S} \tag{23}$$

$$C_{\mathcal{M}_\alpha} = C_{\mathcal{M}_{wb}} - C_{L_{\alpha_W}}\left(\bar{x}_{ac_W} - \bar{x}_{CG}\right) - C_{L_{\alpha_H}}\left(\bar{x}_{ac_H} - \bar{x}_{CG}\right)\left(1 - \frac{\partial \varepsilon}{\partial \alpha}\right)\eta_H \frac{S_H}{S} \tag{24}$$

$$C_{\mathcal{M}_q} = -2.2C_{L_{\alpha_H}}\left(\bar{x}_{ac_H} - \bar{x}_{CG}\right)^2 \eta_H \frac{S_H}{S} \tag{25}$$

Variation of Airplane Pitching Moment Coefficient with Elevator Deflection Angle

$$C_{\mathcal{M}_{\delta e}} = -C_{L_{\alpha_H}}\left(\bar{x}_{ac_H} - \bar{x}_{CG}\right)\eta_H \frac{S_H}{S} \quad (26)$$

Longitudinal Modes

Phugoid mode

The phugoid mode is characterized by a lightly damped low frequency oscillation of an aircraft's forward velocity and pitch angle. If an aircraft is perturbed by a gust of wind and the nose points above the horizon line (increase in pitch angle), there is an inertial component countered by gravity. As the aircraft decreases in speed, lift decreases and the pitch angle reduces. When the nose of the aircraft is below the horizon line, airspeed increases which produces more lift and the response is to nose up. Since the frequency of the oscillation is low, pilots can easily correct with elevator control inputs.

Short period mode

The short period mode is generally characterized by a heavily damped high frequency oscillation of an aircraft's angle of attack (α) and pitch rate (q). In cases when damping or frequency is low, an aircraft's response to elevator response lags a pilot elevator control input. This is characteristic of a poorly controllable aircraft.

Corrected State-Space for Analysis

The correction to the state-space in equation (3) is to use the following small angle approximation.

$$\alpha = \tan^{-1}\left(\frac{w}{U}\right) \approx \frac{w}{U} \rightarrow \quad w = \alpha \cdot U \rightarrow \quad \dot{w} = \dot{\alpha} \cdot U$$

Substituting in the above relation, equation (3) into equation (27).

$$\begin{bmatrix} \dot{u} \\ \dot{\alpha} \\ \dot{q} \\ \dot{\theta} \end{bmatrix} = \begin{bmatrix} X_u & X_w U_1 & 0 & -g \\ Z_u/U & Z_w & 1 & 0 \\ (\mathcal{M}_u + \mathcal{M}_{\dot{w}} Z_u) & (\mathcal{M}_w + \mathcal{M}_{\dot{w}} Z_w) U_1 & (\mathcal{M}_q + \mathcal{M}_{\dot{w}} U_1) & 0 \\ 0 & 0 & 1 & 0 \end{bmatrix} \begin{bmatrix} u \\ \alpha \\ q \\ \theta \end{bmatrix} + \begin{bmatrix} X_{\delta e} \\ Z_{\delta e}/U_1 \\ (\mathcal{M}_{\delta e} + \mathcal{M}_{\dot{w}} Z_{\delta e}) \\ 0 \end{bmatrix} [\delta e] \quad (27)$$

Lateral/Directional Dynamics

The lateral/directional state-space is developed from the equations of motion (2). Since lateral velocity is not a significant parameter for the lateral/directional modes, the following substitution is made in the lateral/directional equations of motions.

$$\beta = \tan^{-1}\left(\frac{v}{U}\right) \approx \frac{v}{U} \rightarrow \quad v = \beta \cdot U, \;\; \dot{v} = \dot{\beta} \cdot U$$

Substituting the above relation for lateral velocity and adding $\dot{\phi} = p$, the lateral/directional state-space is represented by equation (28).

$$\begin{bmatrix} \dot{\beta} \\ \dot{p} \\ \dot{r} \\ \dot{\phi} \end{bmatrix} = \begin{bmatrix} Y_\beta/U_1 & Y_p/U_1 & (Y_r/U_1 - 1) & g/U_1 \\ \left(K_I \cdot \mathcal{L}_\beta + \frac{I_{xz}}{I_{xx}} K_I \cdot \mathcal{N}_\beta\right) & \left(K_I \cdot \mathcal{L}_p + \frac{I_{xz}}{I_{xx}} K_I \cdot \mathcal{N}_p\right) & \left(K_I \cdot \mathcal{L}_r + \frac{I_{xz}}{I_{xx}} K_I \cdot \mathcal{N}_r\right) & 0 \\ \left(K_I \cdot \mathcal{N}_\beta + \frac{I_{xz}}{I_{zz}} K_I \cdot \mathcal{L}_\beta\right) & \left(K_I \cdot \mathcal{N}_p + \frac{I_{xz}}{I_{zz}} K_I \cdot \mathcal{L}_p\right) & \left(K_I \cdot \mathcal{N}_r + \frac{I_{xz}}{I_{zz}} K_I \cdot \mathcal{L}_r\right) & 0 \\ 0 & 1 & 0 & 0 \end{bmatrix} \begin{bmatrix} \beta \\ p \\ r \\ \phi \end{bmatrix} + \begin{bmatrix} 0 & Y_{\delta r}/U_1 \\ \left(K_I \cdot \mathcal{L}_{\delta a} + \frac{I_{xz}}{I_{xx}} K_I \cdot \mathcal{N}_{\delta a}\right) & \left(K_I \cdot \mathcal{L}_{\delta r} + \frac{I_{xz}}{I_{xx}} K_I \cdot \mathcal{N}_{\delta r}\right) \\ \left(K_I \cdot \mathcal{N}_{\delta a} + \frac{I_{xz}}{I_{xx}} K_I \cdot \mathcal{L}_{\delta a}\right) & \left(K_I \cdot \mathcal{N}_{\delta r} + \frac{I_{xz}}{I_{xx}} K_I \cdot \mathcal{L}_{\delta r}\right) \\ 0 & 0 \end{bmatrix} \begin{bmatrix} \delta a \\ \delta r \end{bmatrix} \quad (28)$$

Where,

$$K_I = \frac{I_{xx} \cdot I_{zz}}{I_{xx} \cdot I_{zz} - I_{xz}^2}$$

For cases where $I_{xz} \approx 0$ or $I_{xz} << I_{xx}$ or I_{zz}, equation (28) reduces to equation (29).

$$\begin{bmatrix}\dot{\beta}\\ \dot{p}\\ \dot{r}\\ \dot{\Phi}\end{bmatrix}=\begin{bmatrix}Y_\beta/U_1 & Y_p/U_1 & (Y_r/U_1-1) & g/U_1\\ \mathcal{L}_\beta & \mathcal{L}_p & \mathcal{L}_r & 0\\ \mathcal{N}_\beta & \mathcal{N}_p & \mathcal{N}_r & 0\\ 0 & 1 & 0 & 0\end{bmatrix}\begin{bmatrix}\beta\\ p\\ r\\ \Phi\end{bmatrix}+\begin{bmatrix}0 & Y_{\delta r}/U_1\\ \mathcal{L}_{\delta a} & \mathcal{L}_{\delta r}\\ \mathcal{N}_{\delta a} & \mathcal{N}_{\delta r}\\ 0 & 0\end{bmatrix}\begin{bmatrix}\delta a\\ \delta r\end{bmatrix} \quad (29)$$

Lateral/Directional Derivatives

The lateral/directional derivatives in equations (28) and (29) are mathematically represented with equations (30) through (43) [3] and [4].

Lateral Acceleration per Unit Sideslip

$$Y_\beta=\frac{\bar{q}_\infty\cdot S\cdot C_{Y_\beta}}{m}\left(\frac{ft/sec^2}{rad}\right)or\left(\frac{m/sec^2}{rad}\right) \quad (30)$$

Lateral Acceleration per Unit Roll Rate

$$Y_r=\frac{\bar{q}_\infty\cdot S\cdot b\cdot C_{Y_p}}{2m\cdot U_1}\left(\frac{ft/sec}{rad}\right)or\left(\frac{m/sec}{rad}\right) \quad (31)$$

Lateral Acceleration per Unit Yaw Rate

$$Y_r=\frac{\bar{q}_\infty\cdot S\cdot b\cdot C_{Y_r}}{2m\cdot U_1}\left(\frac{ft/sec}{rad}\right)or\left(\frac{m/sec}{rad}\right) \quad (32)$$

Lateral Acceleration per Unit Rudder Angle Deflection

$$Y_{\delta r}=\frac{\bar{q}_\infty\cdot S\cdot C_{Y_{\delta r}}}{m}\left(\frac{ft/sec^2}{rad}\right)or\left(\frac{m/sec^2}{rad}\right) \quad (33)$$

Roll Angular Acceleration per Unit Sideslip Angle

$$\mathcal{L}_\beta=\frac{\bar{q}_\infty\cdot S\cdot b\cdot C_{\mathcal{L}_\beta}}{I_{xx}}\left(\frac{rad/sec^2}{rad}\right) \quad (34)$$

Roll Angular Acceleration per Unit Roll Rate

$$\mathcal{L}_p=\frac{\bar{q}_\infty\cdot S\cdot b^2\cdot C_{\mathcal{L}_p}}{2I_{xx}\cdot U_1}\left(\frac{1}{sec}\right) \quad (35)$$

Roll Angular Acceleration per Unit Yaw Rate

$$\mathcal{L}_r=\frac{\bar{q}_\infty\cdot S\cdot b^2\cdot C_{\mathcal{L}_r}}{2I_{xx}\cdot U_1}\left(\frac{1}{sec}\right) \quad (36)$$

Roll Angular Acceleration per Unit Aileron Angle Deflection

$$\mathcal{L}_{\delta a}=\frac{\bar{q}_\infty\cdot S\cdot b\cdot C_{\mathcal{L}_{\delta a}}}{I_{xx}}\left(\frac{rad/sec^2}{rad}\right) \quad (37)$$

Roll Angular Acceleration per Unit Rudder Angle Deflection

$$\mathcal{L}_{\delta r}=\frac{\bar{q}_\infty\cdot S\cdot b\cdot C_{\mathcal{L}_{\delta r}}}{I_{xx}}\left(\frac{rad/sec^2}{rad}\right) \quad (38)$$

Yaw Angular Acceleration per Unit Sideslip Angle

$$\mathcal{N}_\beta=\frac{\bar{q}_\infty\cdot S\cdot b\cdot C_{\mathcal{N}_\beta}}{I_{zz}}\left(\frac{rad/sec^2}{rad}\right) \quad (39)$$

Yaw Angular Acceleration per Unit Roll Rate

$$\mathcal{N}_p=\frac{\bar{q}_\infty\cdot S\cdot b^2\cdot C_{\mathcal{N}_p}}{2I_{zz}\cdot U_1}\left(\frac{1}{sec}\right) \quad (40)$$

Yaw Angular Acceleration per Unit Yaw Rate

$$\mathcal{N}_r=\frac{\bar{q}_\infty\cdot S\cdot b^2\cdot C_{\mathcal{N}_r}}{2I_{zz}\cdot U_1}\left(\frac{1}{sec}\right) \quad (41)$$

Yaw Angular Acceleration per Unit Aileron Angle Deflection

$$\mathcal{N}_{\delta a}=\frac{\bar{q}_\infty\cdot S\cdot b\cdot C_{\mathcal{N}_{\delta a}}}{I_{zz}}\left(\frac{rad/sec^2}{rad}\right) \quad (42)$$

Yaw Angular Acceleration per Unit Rudder Angle Deflection

$$\mathcal{N}_{\delta r}=\frac{\bar{q}_\infty\cdot S\cdot b\cdot C_{\mathcal{N}_{\delta r}}}{I_{zz}}\left(\frac{rad/sec^2}{rad}\right) \quad (43)$$

Lateral/Directional Coefficients

The lateral/directional coefficients in equation (30) through (43) are approximated with equations (44) through (57). The lateral/directional coefficients are more difficult to specifically define due to the coupling aircraft dynamics of the roll and yaw. Therefore, higher fidelity solutions would require more accurate expressions for the coefficients. *Note*: The coefficients marked in the title with * or **, are specific to the aircraft geometry and determined from methods presented in [7] for * and [6] for **.

Variation of Airplane Side Force Coefficient with Sideslip Angle

$$C_{Y_\beta} = -C_{L_{\alpha_v}}\left(1-\frac{\partial\sigma}{\partial\beta}\right)\eta_v\cdot\left(\frac{S_v}{S}\right) \tag{44}$$

Variation of Airplane Side Force Coefficient with Dimensionless Change in Roll Rate

$$C_{Y_p} = -2C_{L_{\alpha_v}}\left(\frac{z_{ac_v}-z_{cg}}{b}\right)\eta_v\cdot\left(\frac{S_v}{S}\right) \tag{45}$$

Variation of Airplane Side Force Coefficient with Dimensionless Change in Yaw Rate

$$C_{Y_r} = -2C_{Y_\beta}\left(\frac{x_{ac_v}-x_{cg}}{b}\right) \tag{46}$$

Variation of Airplane Side Force Coefficient with Rudder Angle Deflection

$$C_{Y_{\delta r}} = C_{L_{\alpha_v}}\cdot\eta_v\left(\frac{S_v}{S}\right)\tau_v \tag{47}$$

**Variation of Airplane Rolling Moment Coefficient with Sideslip Angle*

$$C_{\mathcal{L}_\beta} = -0.142C_{L_1} \tag{48}$$

Variation of Airplane Rolling Moment Coefficient with Dimensionless Change in Roll Rate

$$C_{\mathcal{L}_p} = -4C_{L_{\alpha_w}}\frac{1}{S\cdot b^2}\int_0^{b/2} c(y)\cdot y^2\cdot dy \tag{49}$$

**Variation of Airplane Rolling Moment Coefficient with Dimensionless Change in Yaw Rate*

$$C_{\mathcal{L}_r} = 0.2C_{L_1} - 2C_{Y_\beta}\left[\frac{(x_{ac_v}-x_{cg})(z_{ac_v}-z_{cg})}{b^2}\right] \tag{50}$$

Variation of Airplane Rolling Moment Coefficient with Aileron Angle Deflection

$$C_{\mathcal{L}_{\delta a}} = 2C_{L_{\alpha_w}}\frac{\tau_{\delta a}}{S\cdot b}\int_{y_1}^{y_2} c(y)\cdot y\cdot dy \tag{51}$$

Variation of Airplane Rolling Moment Coefficient with Rudder Angle Deflection

$$C_{\mathcal{L}_{\delta r}} = C_{L_{\alpha_v}}\left(\frac{z_{ac_v}-z_{cg}}{b}\right)\left(\frac{S_v}{S}\right)\tau_{\delta r} \tag{52}$$

Variation of Airplane Yawing Moment Coefficient with Sideslip

$$C_{\mathcal{N}_\beta} = C_{\mathcal{N}_{\beta_{wf}}} + C_{L_{\alpha_v}}(x_{ac_v}-x_{cg})\left(\frac{1}{b}\right)\left(\frac{S_v}{S}\right)\eta_v \tag{53}$$

Angle

**Variation of Airplane Yawing Moment Coefficient with Dimensionless Change in Roll Rate*

$$C_{\mathcal{N}_p} = -0.23C_{L_1} \tag{54}$$

Variation of Airplane Yawing Moment Coefficient with Dimensionless Change in Yaw Rate

$$C_{\mathcal{N}_r} = -2C_{L_{\alpha_v}}\left(\frac{x_{ac_v} - x_{cg}}{b}\right)^2\left(\frac{S_v}{S}\right)\eta_v \tag{55}$$

***Variation of Airplane Yawing Moment Coefficient with Aileron Angle Deflection*

$$C_{\mathcal{N}_{\delta a}} = -0.26C_{L_1}\cdot C_{\mathcal{L}_{\delta a}} \tag{56}$$

Variation of Airplane Yawing Moment Coefficient with Rudder Angle Deflection

$$C_{\mathcal{N}_{\delta r}} = -C_{L_{\alpha_v}}\left(\frac{x_{ac_v} - x_{cg}}{b}\right)\left(\frac{S_v}{S}\right)\eta_v\tau_{\delta r} \tag{57}$$

Lateral/Directional Modes

Roll mode

The typical characteristic of the roll mode is a perturbation in the roll-axis. There are two primary problems where roll mode analysis is required, low and high speed. In low speed, such as at approach, an aircraft is flying with a high C_L. Any gust of wind can cause one wing to stall momentarily. This can lead to low damped oscillatory roll mode between each wing stalling and recovering. At high speeds, roll reversal can occur. This is a result of aeroelastic behavior. Deflected ailerons at high speed cause a greater moment about the wing than at low speed. The wing responses by twisting, causing an opposite effect in lift from what the aileron input is trying to accomplish. The aircraft's response is roll opposite of the aileron input. Such analysis requires higher fidelity equations than the ones proposed above due to the rigid body assumption.

Spiral mode

The spiral mode is characterized by a change in bank angle (ϕ) and heading angle (ψ). These changes correlated to changes in sideslip (β), roll rate (p), and yaw rate (r). An aircraft with a stable spiral mode will return to level wing flight after perturbations. A neutral or unstable aircraft will continue to spiral into the ground with a corkscrew trajectory if uncorrected.

Dutch-roll mode

The dutch-roll mode is characterized by an oscillation in sideslip (β), roll rate (p), and yaw rate (r). The typical motion is an exchange between roll and yaw as shown in

Figure **6**. Modern aircraft are designed with yaw damper controllers to reduce workload on pilots to correct for this type of mode.

Figure 6. *Dutch-Roll Motion [2]*

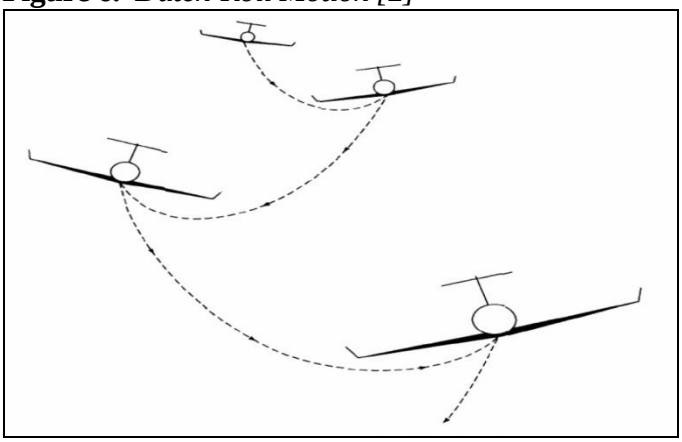

Results

The following longitudinal and lateral/directional responses are the aircraft's reaction to control surface inputs. Similar responses could be due to changing wind directions during flight. These responses are the simple open-loop dynamics of the aircraft with no feedback.

Flight Conditions, Aircraft Geometry, and Stability Coefficients

The AMT's dynamic response is tested at cruise conditions. Primary training exercises for a USAF military trainer occur between 10,000ft (~3,050m) and 18,000ft (~5,485m) [8]. The atmospheric conditions are taken at 4,570m (15,000ft). The other flight conditions used for the simulation are listed in

Table **2**. The aircraft mass parameters used are listed in Table 3. The three aerodynamic surfaces' parameters are listed in Table 4. The aircraft's values listed in Table 3 and Table 4 were determined previously during the design process in [1]. Table 5 lists the calculated longitudinal and lateral/directional coefficients.

Table 2. *Flight Conditions*

Parameter	Value	Units
Flight speed	225	m/s
Mach #	0.7	N/A
Air density	0.769	kg/m^3
Air viscosity	$1.94x10^{-5}$	Pa·s
$\partial\varepsilon/\partial\alpha$	0.536	N/A
$\partial\sigma/\partial\beta$	0.05	N/A
η	0.9	N/A

Table 3. *Aircraft Mass Parameters*

Parameter	Value			Units
x_{cg}	8.03	8.06	8.09	m
z_{cg}	2.0	2.0	2.0	m
Mass	5,320	4,535	3,750	kg
I_{xx}	4,350	3,730	3,115	$kg{\cdot}m^2$
I_{yy}	40,920	39,800	38,640	$kg{\cdot}m^2$
I_{zz}	44,030	42,420	40,770	$kg{\cdot}m^2$

Table 4. *Lifting Surface Parameters*

Component	Parameter	Value	Units	Component	Parameter	Value	Units
Wing	x_{ac}	8.50	m	Aileron	y_1	3.30	m
	Area	18.4	m^2		y_2	4.80	m
	Span	9.60	m		%Chord	20	N/A
	MAC	2.15	m		Area	0.678	m^2
	$C_{L_{\alpha_w}}$	4.52	1/rad		τ_A	0.120	N/A
	AR	5	N/A	Stabilizer	x_{ac}	12.4	m
	e	0.8	N/A		Area	2.51	m_2
Vertical(2)	x_{ac}	10.4	m		Span	2.75	m
	z_{ac}	4.4	m		MAC	0.971	m
	Area	1.82	m^2		$C_{L_{\alpha_w}}$	3.40	1/rad
	Span	3.3	m		AR	3	N/A
	MAC	1.17	m	Rudder	z_1	0.165	m
	$C_{L_{\alpha_w}}$	2.06	1/rad		z_2	3.14	m
	AR	1.5	N/A		%Chord	40	N/A
	Dihedral	15	deg		Area	0.652	m^2
					τ_R	0.640	N/A

Table 5. *Stability Coefficients*

Longitudinal		Lateral/Directional	
Coefficient	**Value**	**Coefficient**	**Value**
C_{D_u}	0.0	C_{Y_β}	-0.353
C_{D_α}	0.109	C_{Y_p}	-0.100
$C_{D_{\delta e}}$	0.398	C_{Y_r}	0.176
C_{D_1}	0.0247	$C_{Y_{\delta r}}$	0.238
$C_{L_{\alpha_{A/C}}}$	4.714	$C_{\mathcal{L}_\beta}$	-0.0206
C_{L_u}	0.145	$C_{\mathcal{L}_p}$	-0.527
$C_{Z_{\delta e}}$	-0.416	$C_{\mathcal{L}_r}$	0.0455
C_{L_1}	0.145	$C_{\mathcal{L}_{\delta a}}$	0.0411
$C_{\mathcal{M}_u}$	-0.0083	$C_{\mathcal{L}_{\delta r}}$	0.0235
$C_{\mathcal{M}_{\dot{\alpha}}}$	-2.286	$C_{\mathcal{N}_\beta}$	0.250
$C_{\mathcal{M}_\alpha}$	-1.404	$C_{\mathcal{N}_p}$	0.0333
$C_{\mathcal{M}_q}$	-4.6689	$C_{\mathcal{N}_r}$	-0.0463
$C_{\mathcal{M}_{\delta e}}$	-0.942	$C_{\mathcal{N}_{\delta a}}$	-0.0016
$C_{\mathcal{M}_1}$	0.0	$C_{\mathcal{N}_{\delta r}}$	-0.0594

Longitudinal Response

Response to Impulse Input of 1^o Stabilator Deflection

The input is a positive one-degree, trailing edge up, stabilator deflection. This results with a downforce from the tail and causes the aircraft to pitch up. This type of input exercises the longitudinal modes of the AMT. The resulting response is shown in Figure 7. The phugoid mode is represented by the left two plots, and the short period by the right two plots.

Figure 7. *AMT Response to 1^o Stabilator Deflection Impulse for Three Loading Conditions*

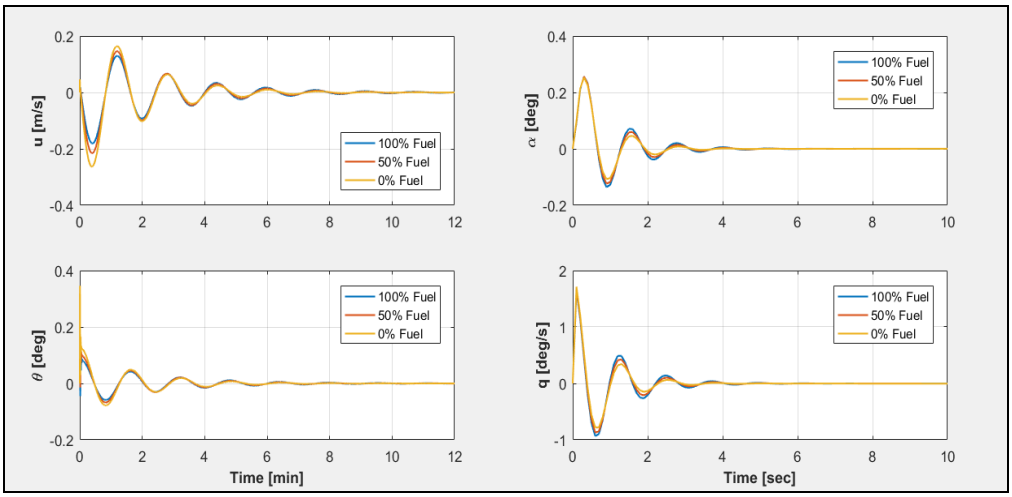

Phugoid impulse response discussion

The AMT's phugoid response is very typical. This lightly damped oscillation of pitch angel (θ) and forward velocity (u) dampen out after about eight minutes as shown in Figure 7. Though not shown in the response, the change in forward velocity and pitch angle also correlate to a change in altitude. The motion of the aircraft would resemble a boat riding the waves in the ocean.

The static margin of the AMT decreases as fuel is burned [1]. This indicates a less stable aircraft but as the response shows, there is not a significant change in the response from fully fueled to being empty. The only noticeable difference is the slight increase in oscillation amplitudes. This can be attributed to the decrease in the aircraft's moment of inertia about the y-axis due to fuel burn. This reduction of mass correlates with a decreased static margin, though not significant to drive the system unstable in this configuration.

Short period impulse response discussion

The AMT's short period response is also very typical. The angle of attack and pitch rate respond with a high frequency oscillation that is heavily damped. The period of the oscillation is about one second, and the AMT returns to its steady-state after about five seconds. Such a response does not require a computerized controller, but modern military aircraft generally employ an augmented control system. Such a system can easily be tailored to reduce the oscillations of these state variables. These types of oscillations cause fatigue stresses in the structure and an augment controller would help to mitigate damage over the lifecycle of the AMT.

Response to Ramp Input to 1^o Stabilator Deflection and Hold

The ramp input response correlates with trimming the aircraft. Trimming the aircraft balances the moments about the cg from the wing and tail. This type of input helps to determine how the aircraft responds to a change in the conditions and how it adjusts to a new steady-state command. The ramp input goes from 0 to 1^o stabilator deflection in a half second.

Figure **8** shows the response of the AMT to ramp input.

Figure 8. *AMT Response to a 1^o Stabilator Deflection Ramp Input for Three Loading Conditions*

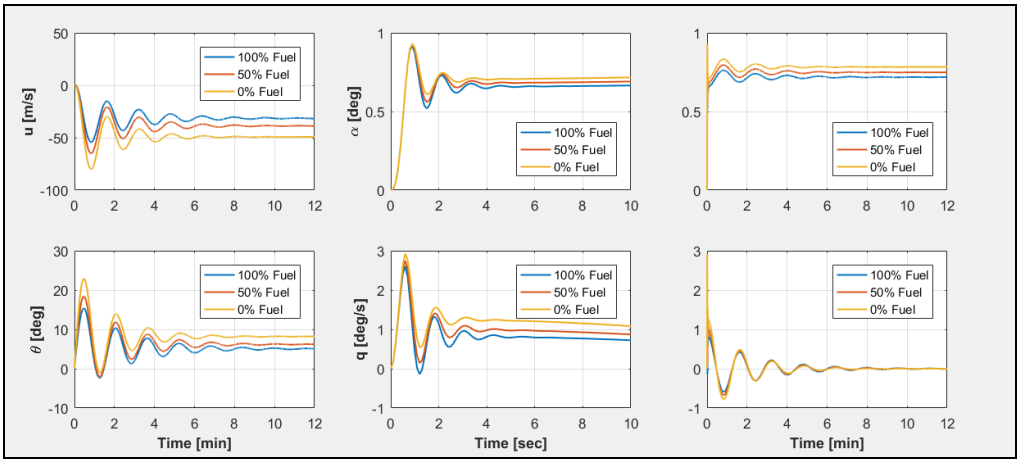

Phugoid ramp and hold response discussion

The phugoid response has a similar characteristic as the impulse response. The difference being the aircraft is now trimmed in a new configuration. A greater negative load on the tail causes the aircraft to rebalance at a higher angle of attack, as seen in the top right plot of

Figure **8**. This correlates to a higher lift coefficient. Therefore, to maintain level flight the dynamic pressure must decrease. Combined with greater drag, the aircraft's new steady-state forward velocity has decreased from its previous steady-state.

The ramp input has a significant effect on pitch angle as compared with the impulse response previously observed. The oscillation magnitude is much greater. This correlates to a significant change in altitude as the aircraft rides through the phugoid mode.

Generally, the angle of attack and pitch rate are not associated with the phugoid mode. From the response, a ramp input creates a significant long period oscillation in these parameters. This response can be seen in the right two plots of

Figure **8**.

The ramp input highlights how the loading conditions have a significant change in the aircraft's response, as compared with an impulse response. The lower loading conditions result with a slightly higher angle of attack correlating to a higher lift coefficient. The aircraft responds with a greater decrease in forward velocity as compared with the fully loaded aircraft. The new steady-state pitch angle settles at 5^{o} to 9^{o} above the horizon line depending on the loading conditions. The oscillations settle at the new steady-state after about 9 to 10 minutes, slightly longer than the impulse response.

Short period ramp and hold response discussion

The short period response to the ramp input is not significantly different than the impulse response. This can be attributed to the high damping observed in this mode. The length of oscillations is also not significantly greater from the impulse response observed.

Lateral/Directional Response

The lateral/directional control surfaces are used for maneuvering and perturbation corrections. There is not the same requirement as the longitudinal controls to trim the aircraft. Though in multi-engine aircraft configurations there is engine out criteria to check for. This is due to the yawing moment due to differential thrust. The AMT is a single engine aircraft and the primary goal of the analysis is to check if the AMT exhibits spiral divergence, roll divergence, or dutch-roll. The response to an aileron deflection impulse is shown in Figure 9 and Figure 10. The response to a rudder deflection impulse is shown in Figure 11 and Figure **12**.

Figure 9. *AMT 90-Second Response to a 1^o Aileron Deflection Impulse for Three Loading Conditions*

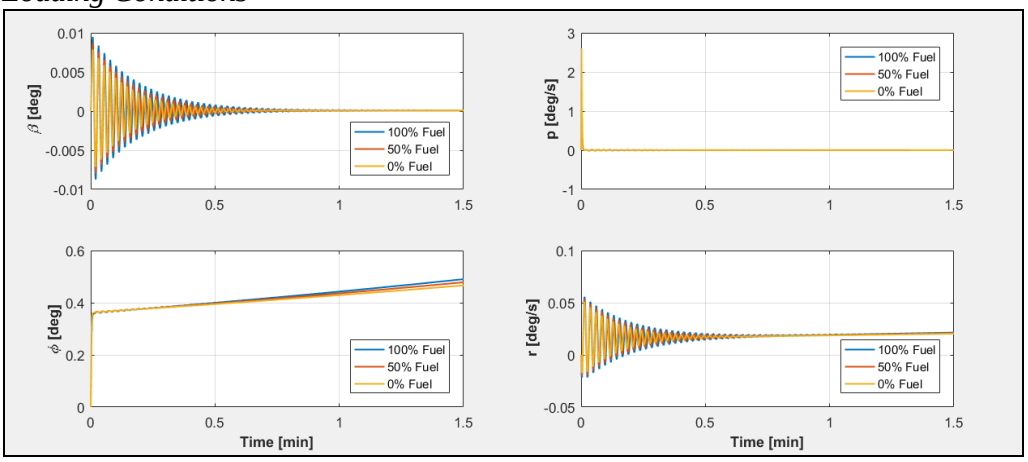

Response to Impulse Input of 1^o Aileron Deflection

Figure 10. *AMT 10-Minute Response to a 1^o Aileron Deflection Impulse for Three Loading Conditions*

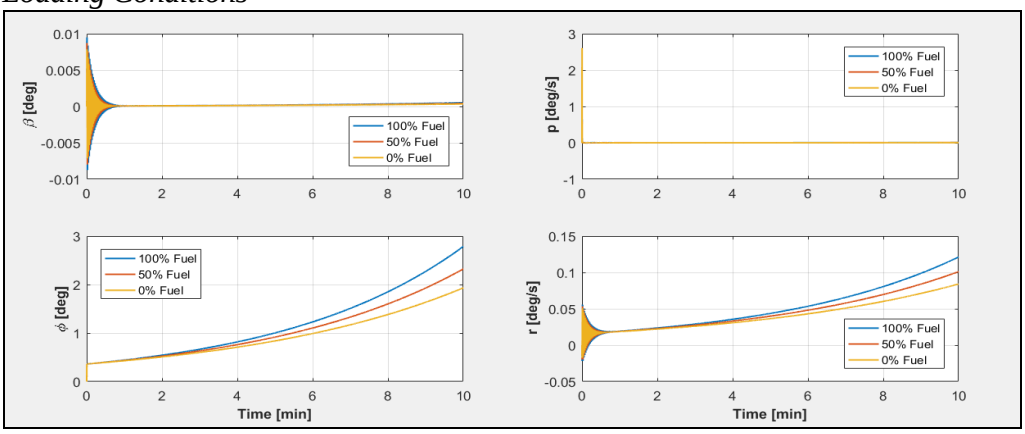

Aileron impulse response discussion

The first note to the aileron impulse is the high frequency oscillation in sideslip angle and yaw rate. This type of oscillation does not correlate to dutch-roll because it is a lower frequency mode similar to the phugoid. This type of response would be corrected to help reduce fatigue damage due to vibrations.

Based on the bank angle (ϕ), the AMT has an unstable spiral mode. There are two possible corrections for this problem. One, employ dihedral in the wings. Two, correct the response with an augmented control system. Also, since modern military aircraft are fly-by-wire, an augmented controller could be a simple fix. Since the AMT is an advanced trainer, maneuverability is desirable and therefore the controller may be the easiest solution. This option would be explored further in a more in-depth stability and control analysis

Based on the roll response, the AMT does not have any roll mode divergence. The different loading configurations do not have a significant impact in the response as compared with the longitudinal response. The noticeable effect is the fully loaded aircraft diverges faster in the spiral.

Response to Impulse Input of 1^o Rudder Deflection

Figure 11. *AMT 90-Second Response to a 1^o Rudder Deflection Impulse for Three Loading Conditions*

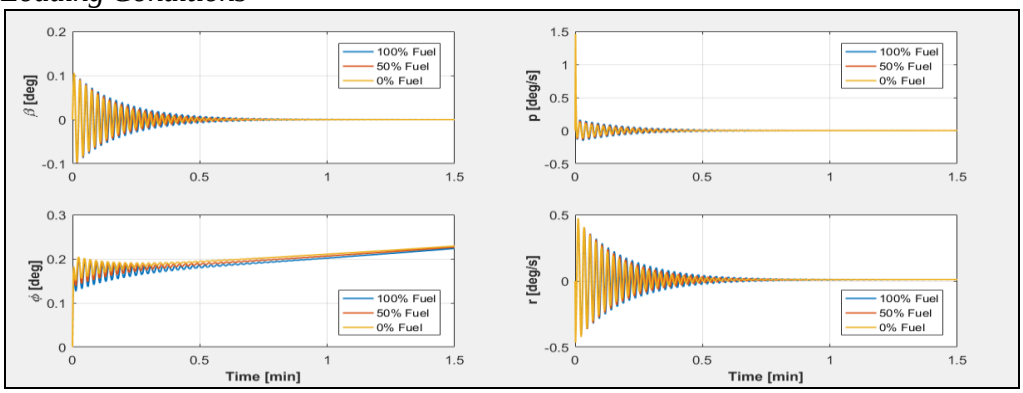

Figure 12. *AMT 10-Minute Response to a 1^o Rudder Deflection Impulse for Three Loading Conditions*

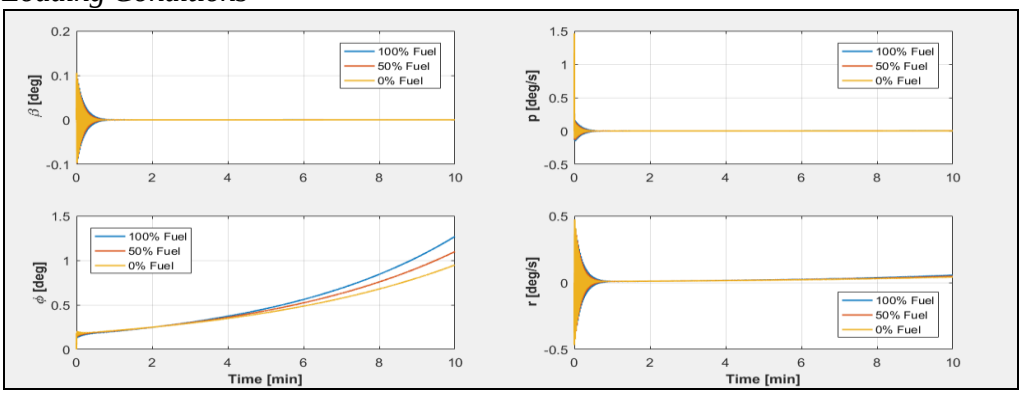

Rudder impulse response discussion

The rudder impulse response is very similar to the aileron response but with smaller magnitudes. The noticeable difference is the high frequency oscillation in roll rate (p) and bank angle (ϕ) in Figure 11. As already mentioned, wing dihedral or an augment controller could be used to correct the spiral divergence.

Conclusions

The longitudinal response analysis demonstrated the AMT is reasonability stable and has acceptable controllability characteristics. Additional analysis that would be of interest is:

- Low speed for landing conditions.
- High-g pull pitch ups and push overs.
- Supersonic flight.

Based on such analysis of various flight conditions, augmented control laws would be developed to tailor the AMT's dynamic response to the specific requirements of the USAF T-X Program.

The lateral/directional response analysis showed there are some stability and control flaws that would need to be corrected if the aircraft went into prototype development and testing. There are high frequency oscillations that could cause fatigue structural failure. The AMT also has a spiral divergent issue which may be corrected with wing dihedral or an augmented control.

References

[1] Johansen, R., *Conceptual Design for a Supersonic Advanced Military Trainer*, San Jose State University, San Jose, California, 2019 (Unpublished).

[2] Roskam, J., (2008), *Airplane Design Parts I – VIII*, DARcorporation, Lawrence, KA., Print.

[3] Nelson, R.C., (1998), *Flight Stability and Automatic Control*, McGraw-Hill, Boston, MA, Print.

[4] Roskam, J., (1995), *Airplane Flight Dynamics and Automatic Flight Controls*, DARcorporation, Lawrence, KS, Print.

[5] Pamadi, B.N., (2015), *Performance, Stability, Dynamics, and Control of Airplanes*, American Institute of Aeronautics and Astronautics, Blacksburg, VA, Print.

[6] Roskam, J., (2008), *Airplane Design Part VI: Preliminary Calculation of Aerodynamic, Thrust and Power Characteristics*, DARcorporation, Lawrence, KA., Print.

[7] Hoak, D.E., et al, (1978) *USAF Stability and Control Datcom*, Flight Control Division, Air Force Flight Dynamics Laboratory, WPAFB, Ohio, Retrieved February 23, 2019 from rahauav.com/Library/Stability-Control/USAF%20DASTCOM_www.rahauav.com.pdf.

[8] FA8617-16-R-6219: System Specification for the Advanced Pilot Training Program, Retrieved September 4, 2018 from https://www.defensedaily.com/wp-content/uploads/post_attachment/ 137563.pdf.